



# Sedimentation of large, soluble proteins up to 140 kDa for $^1\text{H}$ -detected MAS NMR and $^{13}\text{C}$ DNP NMR – practical aspects

Dallas Bell<sup>1,2</sup> · Florian Lindemann<sup>2</sup> · Lisa Gerland<sup>2</sup> · Hanna Aucharova<sup>3</sup> · Alexander Klein<sup>3</sup> · Daniel Friedrich<sup>4</sup> · Matthias Hiller<sup>2</sup> · Kristof Grohe<sup>5</sup> · Tobias Meier<sup>5</sup> · Barth van Rossum<sup>2</sup> · Anne Diehl<sup>2</sup> · Jon Hughes<sup>6,7</sup> · Leonard J. Mueller<sup>8</sup> · Rasmus Linser<sup>3</sup> · Anne-Frances Miller<sup>1,9</sup> · Hartmut Oschkinat<sup>2</sup>

Received: 20 February 2024 / Accepted: 8 May 2024  
© The Author(s) 2024

## Abstract

Solution NMR is typically applied to biological systems with molecular weights < 40 kDa whereas magic-angle-spinning (MAS) solid-state NMR traditionally targets very large, oligomeric proteins and complexes exceeding 500 kDa in mass, including fibrils and crystalline protein preparations. Here, we propose that the gap between these size regimes can be filled by the approach presented that enables investigation of large, soluble and fully protonated proteins in the range of 40–140 kDa. As a key step, ultracentrifugation produces a highly concentrated, gel-like state, resembling a dense phase in spontaneous liquid-liquid phase separation (LLPS). By means of three examples, a *Sulfolobus acidocaldarius* bifurcating electron transfer flavoprotein (*SaETF*), tryptophan synthases from *Salmonella typhimurium* (*SfTS*) and their dimeric  $\beta$ -subunits from *Pyrococcus furiosus* (*PfTrpB*), we show that such samples yield well-resolved proton-detected 2D and 3D NMR spectra at 100 kHz MAS without heterogeneous broadening, similar to diluted liquids. Herein, we provide practical guidance on centrifugation conditions and tools, sample behavior, and line widths expected. We demonstrate that the observed chemical shifts correspond to those obtained from  $\mu\text{M}$ /low mM solutions or crystalline samples, indicating structural integrity. Nitrogen line widths as low as 20–30 Hz are observed. The presented approach is advantageous for proteins or nucleic acids that cannot be deuterated due to the expression system used, or where relevant protons cannot be re-incorporated after expression in deuterated medium, and it circumvents crystallization. Importantly, it allows the use of low-glycerol buffers in dynamic nuclear polarization (DNP) NMR of proteins as demonstrated with the cyanobacterial phytochrome Cph1.

**Keywords** Protein NMR · Dense phase · Ultracentrifugation · Magic-angle-spinning · Solid-state NMR

✉ Anne-Frances Miller  
afmill3r2@gmail.com

✉ Hartmut Oschkinat  
oschkinat@fmp-berlin.de

<sup>1</sup> Faculty II-Mathematics and Natural Sciences, Technische Universität Berlin, Straße des 17. Juni 135, 10623 Berlin, Germany

<sup>2</sup> Leibniz-Forschungsinstitut für Molekulare Pharmakologie, Robert-Rössle-Str. 10, 13125 Berlin, Germany

<sup>3</sup> Department of Chemistry and Chemical Biology, TU Dortmund University, Otto-Hahn-Str. 4a, 44227 Dortmund, Germany

<sup>4</sup> Department of Chemistry and Biochemistry, University of Cologne, Greinstr. 4, 50939 Cologne, Germany

<sup>5</sup> Bruker BioSpin GmbH & Co. KG, Rudolf-Plank-Str. 23, 76275 Ettlingen, Germany

<sup>6</sup> Institute for Plant Physiology, Justus Liebig University, Senckenbergstr. 3, 35360 Gießen, Germany

<sup>7</sup> Department of Physics, Free University of Berlin, Arnimallee 14, 14195 Berlin, Germany

<sup>8</sup> Department of Chemistry, University of California - Riverside, Riverside, CA 92521, USA

<sup>9</sup> Department of Chemistry, University of Kentucky, Lexington, KY 40506, USA

## Introduction

The majority of soluble proteins, nucleic acids and their complexes targeted in biomedical research exceed 40 kDa in mass, which is larger than what solution NMR can readily undertake whilst still be considered too small for MAS NMR that delivers three-dimensional structures of much larger entities (Jehle et al. 2010; Loquet et al. 2012). Yet, the internal dynamics and molecular associations of these biological macromolecules are as important as their static structures, so it is critical to have robust, generally applicable NMR tools that address all three aspects — independently of sample nature and size. This is especially relevant when drug targets are an urgent focus of the investigation. There are many obstacles when investigating proteins in the 40–110 kDa size range such as spectral complexity, fast transverse relaxation of signals from atoms that are key in assignment procedures and — most importantly — the difficulties in reestablishing protons at exchangeable sites after expression in D<sub>2</sub>O-dissolved medium. Most current solution NMR approaches to large proteins include sparse labeling, often of selected residues, that can yield non-overlapping spectra even if samples are composed of so many

residues that a full spectrum would be uninterpretable. In other approaches, signals in large proteins are kept narrow *via* exploitation of TROSY effects for methyl group spin systems (Tugarinov et al. 2003; Bolik-Coulon et al. 2023). Furthermore, the incorporation of fluorinated aromatic amino acids provides selectivity and exploits the enlarged dispersion of <sup>19</sup>F chemical shifts (Huestis and Raftery 1975; Luck and Falke 1991; Gronenborn 2022). However, these approaches are restrictive regarding amenable residues and provide only local information. For interaction studies and potentially also structural studies, of subunits or in conjunction with the application of AlphaFold (Jumper et al. 2021), methodologies that allow use of the resonances of all amino acids are more desirable. Concepts for achieving at least partial sequence-specific resonance assignments in large proteins by MAS NMR exist (Retel et al. 2017), and the prospects of recent automated assignment software (Klukowski et al. 2023) promise solutions for the large combinatorial problem that occurs when assigning the NMR signals of a 60 kDa protein.

A suitable experimental perspective towards the collection of NMR data for this class of biomolecules is given by MAS of soluble proteins after sedimentation, first applied to obtain resolved NMR spectra of very large oligomeric systems (> 300 kDa) such as  $\alpha$ B-crystallin (Mainz et al. 2009) and  $\alpha$ -Ferritin (Bertini et al. 2011, 2012, 2013). Subsequent experiments with concentrated human superoxide dismutase showed that this approach works also for smaller proteins (Fragai et al. 2013). Later, Stöppler et al. demonstrated the potential of the approach for structural investigations of small proteins by sedimenting the fully protonated, 42 kDa extracellular domain of the neonatal Fc receptor (FcRn<sub>ECD</sub>) which cannot be produced in deuterated form (Stöppler et al. 2018). Without deuteration at the non-exchangeable sites, well-resolved <sup>1</sup>H-<sup>15</sup>N correlations (Bodenhausen and Ruben 1980) were obtained *via* cross polarization (CP) (Paulson et al. 2003; Zhou and Rienstra 2008) after sedimenting the protein into the MAS NMR rotor by ultracentrifugation. Sets of 3D NMR spectra suitable for achieving resonance assignments could be obtained at 100 kHz MAS. The protein's structural integrity and thus the validity of the approach were demonstrated by the similarity of the <sup>1</sup>H-<sup>15</sup>N INEPT-based HSQC recorded on a  $\mu$ M/low mM solution, henceforth called 'dilute', with the corresponding MAS NMR spectrum recorded with a CP-based sequence (Fig. 1). The character of the CP spectrum is similar to that of the solution NMR spectrum through the absence of heterogeneous broadening that is characteristic for amorphous samples.

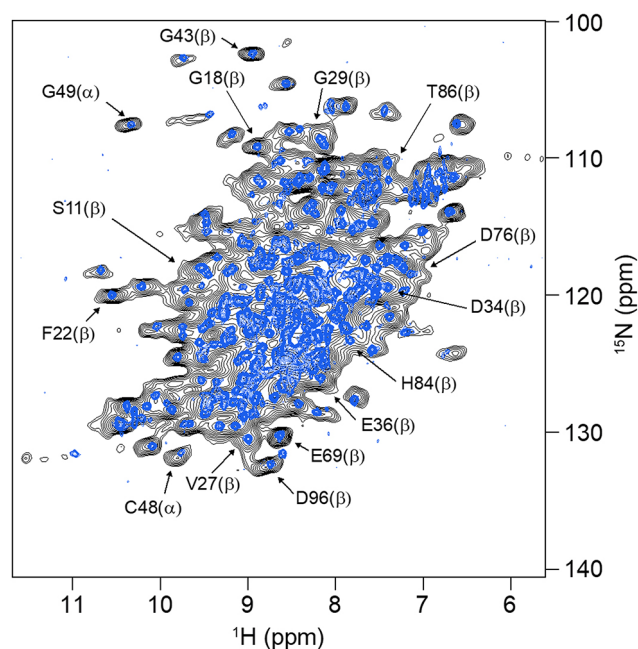


**Fig. 1** <sup>1</sup>H-<sup>15</sup>N NMR correlations of the <sup>13</sup>C, <sup>15</sup>N-labelled extracellular domain of human neonatal Fc receptor recorded in solution (blue spectrum) using an HSQC pulse sequence and at 100 kHz MAS (black spectrum) by cross polarization. Examples of resonance assignments (BMRB entry 27,437 (Stöppler and Oschkinat 2018) based on triple-resonance NMR experiments are indicated for the  $\alpha$ -chain ( $\alpha$ ) and the  $\beta$ 2-microglobulin ( $\beta$ ) subunits of the heterodimeric extracellular domain of the receptor (Stöppler et al. 2018)

In a study on the longevity of MAS NMR samples containing sedimented protein together with small ligands and oligonucleotides, Wiegand et al. applied this concept to a set of larger proteins or their large subunits comprising a bacterial helicase, a polymerase, a primase and an ABC transporter, by employing  $^{13}\text{C}$ -detection in 3.2 mm rotors (Wiegand et al. 2020). In all these cases, the complexes remained intact, as no signs of sample heterogeneity were detected after several years of storage in rotors and repeated MAS NMR experiments. Yet, a layer of gel-like sample was found at the rotor walls, indicating that the gel-like solution present in the rotor prior to experiments had changed to an even denser phase.

There was an early debate regarding the mechanisms that lead to resolved MAS spectra of large dissolved proteins, summarized in Sarkar et al. 2016. One hypothesis states the importance of buffer viscosity and hence temperature as originally outlined in the seminal FROSTY paper (Mainz et al. 2009), whilst another hypothesis attributes the protein immobilization to ‘sedimentation’ processes, as demonstrated by a MAS-dependent CP-transfer in experiments on an apoferritin solution (Bertini et al. 2011). Based on experiments with deep eutectic solvents, Sarkar argues that viscosity and sedimentation can work in tandem (Sarkar et al. 2016). Such deep eutectic solvents consist of small molecules that form networks of interchanging hydrogen bonds or other interactions as is also expected between protein molecules in dense protein phases.

In the current work, we provide a synthesis of these two seemingly different explanations by showing that ultracentrifugation of the protein into the rotor produces a dense protein phase with very high viscosity. Due to the higher  $g$ -values during MAS, further sedimentation takes place in the rotor. In this manner, samples of proteins in the 40–140 kDa range that are suitable for MAS NMR can be generated in a systematic manner by an ultracentrifugation procedure.

This approach is widely applicable and even for non-deuterated proteins, resolved  $^1\text{H}$ - $^{15}\text{N}$  correlations and 3D spectra are obtained at 100–110 kHz MAS from the produced dense phase. With the example of the *Sa*ETF we demonstrate that nitrogen line widths in the 20–30 Hz range can be achieved, and sample lifetimes extend over many weeks. By means of the two tryptophan synthase samples (tetrameric and  $\beta$ -subunit dimers) we demonstrate sample stability and sensitivity, enabling the acquisition of data sets for resonance assignments and distance restraints. In all cases, we provide evidence of close similarity of the  $^1\text{H}$ - $^{15}\text{N}$  correlations recorded on sedimented samples with those obtained from dilute solutions or from crystals as a proof of sample integrity. Importantly, more

complete spectra are obtained than by solution NMR of deuterated proteins, in which signals are often missing due to insufficient back-exchange of amide protons. Furthermore, we demonstrate by means of the example of the phytochrome Cph1 that useful 1D  $^{13}\text{C}$  NMR spectra may be obtained and that this approach is suitable for minimizing freezing-associated formation of ice crystals in MAS DNP NMR (Hall et al. 1997; Barnes et al. 2008) samples with very low levels of glycerol. In such DNP NMR experiments, freeze concentration of the polarizing agent must be avoided to ensure long lifetimes of electron spin states and thus NMR signal enhancements. Usually, this is achieved by adding significant amounts of glycerol to induce a glass-like state upon freezing (Hall et al. 1997). In the case of the phytochrome Cph1 we demonstrate that the glycerol content of the sample could be reduced to about 10%. The procedure ensures substantial signal enhancements attainable via DNP at 800 MHz  $^1\text{H}$  NMR frequency.

## Materials and methods

### Neonatal Fc receptor

The procedure of sample preparation and NMR data acquisition for the extracellular domain of the neonatal Fc receptor (FcRn<sub>ECD</sub>) is described in Stöppler et al. 2018. In brief, a FcRn<sub>ECD</sub>-stable mammalian cell line (HEK293 cells) was generated by transfection and subsequent culture expansion. Cultures with positive FcRn<sub>ECD</sub> expression were selected based on analysis by Western Blotting. The highest expressing pool was expanded to 10 L in a bioreactor, and expression was performed for 10 days in Bioexpress 6000 media (Cambridge Isotope Laboratories) for isotopic labeling. The protein purification protocol is based on affinity chromatography using a KappaSelect (GE Healthcare) column, which had been preloaded with an IgG4 monoclonal antibody to bind FcRn<sub>ECD</sub>, followed by gel filtration with a Superdex 200 (GE Healthcare) column. Elution and peak fractions were analyzed by SDS-PAGE before pooling. The  $^1\text{H}$ - $^{15}\text{N}$  NMR correlation experiment of sedimented FcRn<sub>ECD</sub> was performed on a Bruker AVANCE III 850 MHz spectrometer at 100 kHz MAS with a triple-resonance 0.7 mm MAS probe (Bruker) using cross polarization. Tangential shapes of 40–60% on the  $^1\text{H}$  channel and RF-fields of 93 kHz and 17 kHz were used for  $^1\text{H}$  and  $^{15}\text{N}$ , respectively, to achieve magnetization transfers. Hard pulses of 150 kHz ( $^1\text{H}$ ) and 62.5 kHz ( $^{15}\text{N}$ ) were applied. Acquisition times of 70 ms at a spectral width of 46.68 kHz in F1 and of 16.4 ms at 110 kHz spectral width in F2 were chosen.  $^1\text{H}$ -decoupling was achieved by 10 kHz fslp-TPPM. 32 scans with an

interscan delay of 1.0 s were recorded, resulting in a total acquisition time of about 3 h. The solution-state 2D  $^{15}\text{N}$ - $^1\text{H}$  spectrum was acquired from a 0.35 mL sample of 300  $\mu\text{M}$  [ $^{13}\text{C}$ ,  $^{15}\text{N}$ ]-labeled FcRn<sub>ECD</sub> at 35 °C on a Bruker AVANCE III HD 600 MHz spectrometer equipped with a cryogenically cooled probe. The spectrum was acquired for 40 min with acquisition times of 40 ms for  $^{15}\text{N}$  and 60 ms for  $^1\text{H}$ . Both spectra were processed using Topspin 3.5 (Bruker Biospin). Chemical shift assignments are deposited at the BMRB (Hoch et al. 2023) under the code 27,437 (Stöppler and Oschkinat 2018).

## SaETF

SaETF was expressed from a codon-optimized version of the gene AHC50813.1 (GenBank) synthesized by GenArt Germany and cloned into a pET-derived vector, by using a modular cloning kit (similar to golden gate assembly). The plasmid was transformed into *E. coli* BL21(DE3) cells selected with kanamycin. Expression was induced using isopropyl  $\beta$ -D-thiogalactopyranoside (IPTG) at OD<sub>600</sub> 0.8. After 18 further hours at 18 °C, cells were harvested, washed and frozen at -80 °C until needed. For uniformly labeled  $^{15}\text{N}$ -SaETF, the construct was expressed in M9 medium, including 2 g/L  $^{15}\text{NH}_4\text{Cl}$  culture. Protein purification employed Ni-NTA affinity chromatography. The steps for producing deuterated  $^{15}\text{N}$ -SaETF are the same as above except all chemicals and additives were prepared in 100% D<sub>2</sub>O and 2.5 g/L  $^2\text{H}$ -labelled glucose as sole carbon source was employed. Purification of SaETF began by resuspending cell pellets in lysis buffer (20 mM TRIS/HCl, 500 mM KCl, 10 mM imidazole at pH 7.8) and five cycles in a microfluidizer (LM10, Microfluidics, Newton, MA, USA). The lysate was centrifuged (30 min, 48,384 g) and supernatant was pushed through a 0.45  $\mu\text{m}$  syringe filter. The remaining solution was loaded onto a column of an Äkta Purifier (GE Healthcare), containing Ni-NTA beads (Sigma-Aldrich 70666-4), pre-equilibrated with the lysis buffer. After washing the column, the protein was eluted with 150

mM imidazole. The purification for the deuterated sample occurred in fully protonated buffers. The yield for the  $^{15}\text{N}$ ,  $^1\text{H}$  sample was 16 mg/L; the yield for the  $^{15}\text{N}$ ,  $^2\text{H}$  sample was 33 mg/L. Oligomers were removed by a Superdex200 size exclusion chromatography column mounted on an Äkta FPLC system (GE Healthcare). The protein was subsequently stored in buffer comprising 20 mM TRIS/HCl, 100 mM KCl at pH 7.8. The same buffer was used for the solution NMR measurements after adding 10% D<sub>2</sub>O. For solid-state NMR measurements, the  $^{15}\text{N}$ -labelled protein was sedimented into a 0.7 mm ZrO<sub>2</sub> rotor as specified in Table 1. All measurements were conducted on a Bruker Avance NEO spectrometer operating at 900 MHz  $^1\text{H}$  Larmor frequency. Water suppression was achieved with the MISSISSIPPI sequence for solid-state NMR and the WATERGATE sequence in solution. Decoupling was always achieved by WALTZ16 ( $^1\text{H}$ ,  $^{13}\text{C}$ ,  $^{15}\text{N}$ ). All solid-state NMR spectra were acquired at 100 kHz MAS. A detailed listing of experimental parameters can be found in Tables S1, S2, and S3.

The water content of the sample was roughly estimated on the basis of the integrated 1D  $^1\text{H}$  NMR spectra shown in Fig. S1. The integral of the region between 4.2 and 6 ppm was considered to reflect largely water, and the areas to the right and left protons of the protein. Protein signals under the water lead to an error, yet the water line had a hump extending towards 3 ppm, leading to an error in the opposite direction. We assumed a compensation of both. For the fresh sample, the integral of the water area is 3.8 times larger than the sum of the other two that are reflecting the protein. Since we are interested in the water/protein ratio, it is fair to assume that the protein integral reflects 4862 protons (for one molecule), and the water signal contains 2 protons times x molecules. With an integral ratio of 3.8 and molecular weights of 66,843 g/mol for the protein and 18 g/mol for water a 2.5-fold excess of water (w/w) is obtained.

**Table 1** Parameters relevant for the sedimentation procedure

| Sample              | Mol. weight (kDa) | Rotor (mm) | Conc. ( $\mu\text{M}$ ) | Force (x1000g) | Temp. (K) | Centrifugation Time (h) |
|---------------------|-------------------|------------|-------------------------|----------------|-----------|-------------------------|
| Cph1-WIRV           | 59                | 1.9        | 1700                    | 71             | 278       | 67                      |
| Cph1-PCB            | 59                | 1.9        | 1000                    | 71             | 278       | 68                      |
| FcRn <sub>ECD</sub> | 42                | 0.7        | 100                     | 100            | 277       | 40                      |
| SfTS                | 144               | 0.7        | 140                     | 71             | 281       | 42                      |
| SaETF               | 67                | 0.7        | n.d.                    | 82             | 278       | 70                      |
| <i>Pf</i> TrpB      | 85                | 0.7        | 340                     | 71             | 298       | 94                      |
| <i>Pf</i> TrpB      | 85                | 1.3        | 450                     | 210            | 298       | 72                      |

For each sample, the molecular weight, the outer diameter of the rotor that was filled and the concentration prior to the ultracentrifugation are given in the first three columns, respectively. The centrifugation itself is characterized by the maximum relative gravitational force and temperature during the centrifugation together with the total centrifugation time. n.d.: not determined; Cph1-WIRV: Cph1 solely  $^{13}\text{C}$ ,  $^{15}\text{N}$ -labeled in Trp, Ile, Arg and Val; Cph1-PCB: only the cofactor is  $^{13}\text{C}$ ,  $^{15}\text{N}$ -labeled. *Pf*TrpB bears the mutations I16V, E17G, I68V, F95L, F274S, T292S, T321A, V384A as compared to the wildtype



## StTS

Protein expression was as described in (Caulkins et al. 2016). The  $^{13}\text{C}$ ,  $^{15}\text{N}$ -labeled protein was kept in 50 mM Caesium bicine buffer, pH 7.8, in the presence of 3 mM N-(4'-trifluoromethoxybenzenesulfonyl)-2-aminoethyl phosphate (usually termed F9; a high affinity alpha site ligand). 50  $\mu\text{L}$  of 20 mg/mL protein were sedimented into a 0.7 mm  $\text{ZrO}_2$  rotor with the conditions specified in Table 1. The NMR measurements were conducted on a Bruker Avance NEO spectrometer operating at 900 MHz  $^1\text{H}$  Larmor frequency and at 100 kHz MAS. Water suppression was achieved with the MISSISSIPPI sequence and decoupling by sTPPM ( $^1\text{H}$ ) and WALTZ16 ( $^{13}\text{C}$ ,  $^{15}\text{N}$ ). A detailed overview of experimental NMR parameters can be found in Tables S4 and S5.

## PfTrpB

*P. furiosus* tryptophan synthase b-subunit (*PfTrpB*) was used as the 2B9 variant, containing the mutations I16V, E17G, I68V, F95L, F274S, T292S, T321A, V384A (Buller et al. 2015), which was previously codon-optimized for *E. coli* and cloned into a pET22(b)+ vector with an uncleavable C-terminal 6xHis tag. Two different samples were produced, one being protonated according to the iFD procedure (Medeiros-Silva et al. 2016) and one being  $^2\text{H}$ ,  $^{13}\text{C}$ ,  $^{15}\text{N}$ -triple-labeled and proton back-exchanged (called DCN in the following). Accordingly, two different protocols of expression were used.

Expression procedures for the iFD sample: A single colony of *E. coli* BL21 (DE3) carrying the vector encoding *PfTrpB* was used to inoculate a 5 mL culture of LB media with 100  $\mu\text{g}/\text{mL}$  carbenicillin and incubated overnight at 37 °C at 180 rpm. A 500  $\mu\text{L}$  aliquot was used to inoculate 1 L of M9 media supplemented with  $^{13}\text{C}$ -Glucose, 1, 2, 3, 4, 5, 6, 7- $\text{d}_7$ , (2 g/L),  $^{15}\text{NH}_4\text{Cl}$  (0.5 g/L),  $^2\text{H}$ ,  $^{13}\text{C}$ ,  $^{15}\text{N}$ -labeled ISOGRO (Sigma-Aldrich) algal extract (2 g/L), and carbenicillin (100 mg/L) and incubated at 180 rpm and 37 °C until the  $\text{OD}_{600}$  reached 1. Cultures were chilled on ice for 20–30 min and expression was induced by the addition of IPTG to a final concentration of 1 mM. Cells continued to grow at 180 rpm and 20 °C for another 20 h. Cells were harvested by centrifugation at 4 °C and 4,000 g for 20 min; the pellets were frozen at -80 °C until further use.

Expression procedures for the DCN sample: A single colony of *E. coli* BL21 (DE3) was used to inoculate a 5 mL culture of LB media with 100  $\mu\text{g}/\text{mL}$  carbenicillin (LBcarb) and incubated overnight at 37 °C at 180 rpm. A 500  $\mu\text{L}$  aliquot was used to inoculate 50 mL M9 media in  $\text{H}_2\text{O}$ . Three steps of adaptation to  $\text{D}_2\text{O}$  were performed as followed: (1) 500  $\mu\text{L}$  of M9/ $\text{H}_2\text{O}$  culture was used to inoculate 50 mL of a composite media 10% M9/ $\text{D}_2\text{O}$ , 90% M9/ $\text{H}_2\text{O}$  followed

by incubation for 4 h in shaker; (2) 500  $\mu\text{L}$  of composite culture was inoculated in 50 mL of 50% M9/ $\text{D}_2\text{O}$ , 50% M9/ $\text{H}_2\text{O}$ ; (3) 500  $\mu\text{L}$  of culture was inoculated in 50 mL of 90% M9/ $\text{D}_2\text{O}$ , 10% M9/ $\text{H}_2\text{O}$ . The final culture was transferred to 1 L of M9/ $\text{D}_2\text{O}$  media supplemented with  $^2\text{H}$ ,  $^{13}\text{C}$ ,  $^{15}\text{N}$ -labeled ISOGRO algal extract (2 g/L culture), carbenicillin (100 mg/L) and incubated at 180 rpm and 37 °C until  $\text{OD}_{600}$  reached 1. Induction of protein expression and cell harvest were performed identically to the iFD sample.

Frozen cell pellets were thawed at room temperature and resuspended in buffer A (50 mM phosphate buffer, pH 8.0, with 20 mM imidazole and 100 mM NaCl) supplemented with 200  $\mu\text{M}$  PLP, 1 mM PMSF, 1 mM TCEP, 1 mg/mL hen egg white lysozyme, and 0.02 mg/mL DNase. After vortexing, cells were lysed with an Emulsiflex C3 (Avestin Europe, Mannheim, Germany, three runs for each culture). Lysates were aliquoted into 45 mL tubes and centrifuged at 100,000 g and 4 °C for 20 min, then incubated at 75 °C for 10 min and spun again. The clarified, heat-treated lysate was applied to a 5 mL Ni-NTA column (Macherey-Nagel, Düren, Germany). The protein was eluted by gravity with buffer B (50 mM phosphate buffer pH 8.0, 500 mM Imidazole, 100 mM NaCl). Appropriate fractions were combined and exchanged into NMR buffer (50 mM phosphate buffer pH 8.0, 1 mM TCEP) using a PD10 column (Cytiva Europe, Freiburg, Germany), frozen in liquid  $\text{N}_2$ , and stored at -80 °C until further use. The final yield of *PfTrpB* from 1 L of triple-labeled M9 media was 3.9 mg, and the yield of the iFD sample was around 6 mg. Sedimentation of the iFD sample into a 0.7 mm rotor was achieved by centrifugation for 94 h using a Beckmann SW 40 Ti rotor at 71,100 g and 20 °C. Sedimentation of the DCN sample into a 1.3 mm rotor was achieved by centrifugation for 72 h at 210,000 g and 20 °C.

Solid-state experiments for determining  $^1\text{H}$  bulk sensitivities were recorded on a Bruker Avance NEO 700 MHz ( $^1\text{H}$  Larmor frequency) spectrometer either using a 1.3 mm rotor at an MAS frequency of 55.5 kHz or using an 0.7 mm rotor at 100 kHz MAS. Experiments were recorded using 256 scans to obtain an adequate signal-to-noise ratio (S/N) with a recycle delay 1.3-fold the measured  $T_1$  times ( $^1\text{HN}$  bulk). The intensities represent the first FID of each nD experiment, i.e. using a 200 ns delay for each  $t_n/2$  period and including all necessary pulses for (selective) decoupling. The S/N was determined in Topspin using the same signal and noise region for a given sample. A detailed listing experimental parameters can be found in SI Tables S6–S9.

## Cyanobacterial phytochrome Cph1 from *Synechocystis*

The plasmid p926.5 encoding Cph1 $\Delta$ 2 (the N-terminal NTS-PAS-GAF and PHY domains of Cph1 residues 0-514 with a C-terminal 6xHis tag) was cotransformed with pSE111 encoding for *lacI<sub>q</sub>* and *ArgU* into *E.coli* BL21 DE3 cells using a standard heat shock protocol. A 30 mL preculture was grown for 1 h at 37 °C, 170 rpm on LB medium containing kanamycin (40  $\mu$ g/mL) and carbenicillin (60  $\mu$ g/mL). Cells were spun down (RT, 10 min, 2000 g) and resuspended in 15 mL 2x M9 medium (D<sub>2</sub>O, Glucose, NH<sub>4</sub>Cl). Cells were grown overnight at 32 °C, 170 rpm. Glucose and NH<sub>4</sub>Cl were added and cells kept at 37 °C for 1 h. Then, after reaching an OD<sub>600</sub> of 4.7 (after about 1 h at 18 °C, 170 rpm), protein expression was induced with 100  $\mu$ M IPTG. During expression, Glucose and NH<sub>4</sub>Cl were added when glucose and ammonium chloride levels approached zero. Quantities were measured by commercially available strip tests (Merck, Darmstadt, Germany; Glucose Test MQuant and Ammonium Test). A total amount of 8 g/L glucose and 3 g/L ammonium chloride was used. After 48 h cells were harvested at 18 °C, 2000 g, washed in 150 mM NaCl and stored at -80 °C. For the final steps such as binding of PCB chromophore and photoconversion into the PR-form standard protocols were applied (Essen et al. 2008; Hughes 2010). A non-protein labelled Cph1 $\Delta$ 2 sample was assembled with <sup>1</sup>H, <sup>13</sup>C and <sup>15</sup>N-labelled PCB. 15 mg of Cph1 $\Delta$ 2 in 50 mM Na/PO<sub>4</sub> buffer (pH 7.8, 20% D<sub>2</sub>O) were filled into a 1.9 mm rotor via ultracentrifugation for 68 h, 4 °C, 71,000 g.

1D hC-CP spectra were recorded with 1536 complex points, 16,324 scans, an <sup>13</sup>C acquisition time of 15 ms and a spectral width of 81.5 kHz. For CP, constant <sup>1</sup>H rf-field of 80 kHz was applied while the <sup>13</sup>C spin-lock pulse was ramped from 40 to 50 kHz. The CP contact time was set to 2000  $\mu$ s. During acquisition 100 kHz SPINAL-64 (Fung et al. 2000) proton decoupling was applied. The recycle delay was set to 2 s.

## Results and discussion

### The preparation procedure

The quality of the NMR measurements described below is critically dependent on the sample preparation protocol that produces a dense phase by ultracentrifugation (Table 1; Fig. 2). In the major step, the protein is concentrated by centrifugation at 70 000–85 000 g for a time of 2–3 days at maximum. This time is considered appropriate for proteins in the 40–60 kDa range, ensuring that they are quantitatively

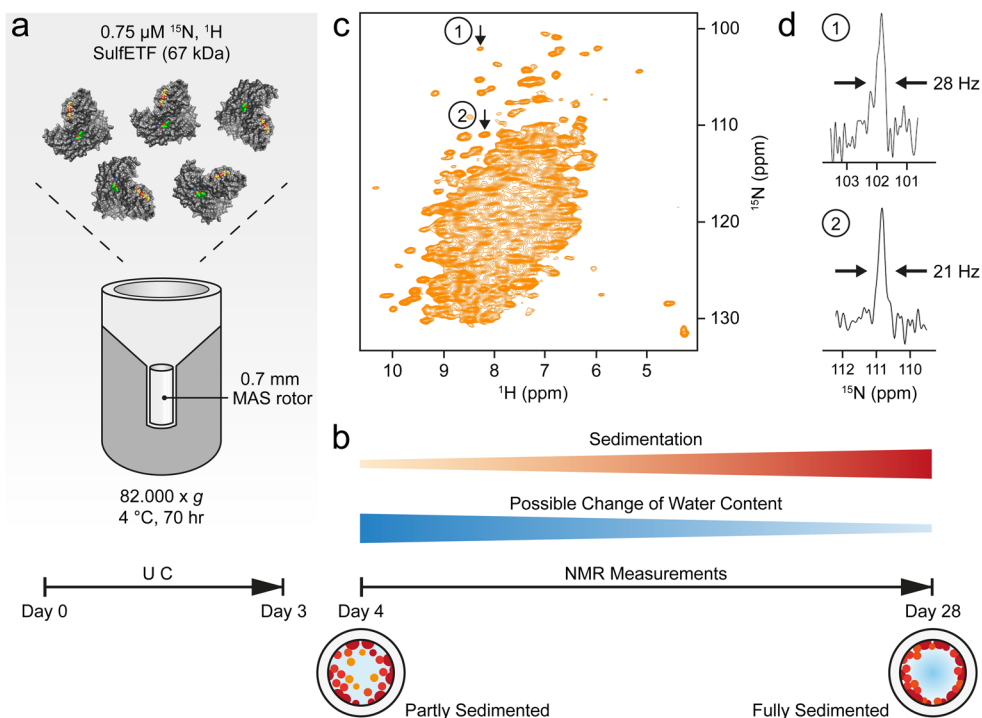
sedimented. Very likely, many larger proteins can be spun down in a shorter period. Calculation of an appropriate centrifugation time is difficult since important factors are the strength and number of the weak interactions between the molecules that become relevant at these very high concentrations and determine the tendency of protein network formation, but which vary depending on the particular protein investigated.

The protein is either directly spun into the rotor (Fig. 2a), or centrifuged into a rotor after concentration of the protein in a separate centrifugation step from which only the concentrated phase is retained. In both cases, a residual dilute ‘buffer’ phase and the dense phase remain separate and can be clearly distinguished from each other. When using small rotors (e.g., 0.7 mm), a filling tool is required for which the engineering drawings are shown in Figs. S2 and S3. A 0.7 mm rotor can contain up to 600 nL of material, whereas the funnel of the filling tool accommodates 250  $\mu$ L (Fig. S2 and S3), so loading the funnel with an initial concentration of 1–4 mg/mL protein yields sufficient amounts of protein in the rotor after centrifugation. Table 1 lists the conditions applied to prepare the samples mentioned in this work. The conditions may also be applied to fill rotors with other diameters, using an adapted filling tool.

In case of *Sa*ETF (Fig. 2a) the ratio of protein-to-water approached 1:2.5 (w/w) (Fig. S1). At that point, the sample is gel-like, often not amenable to transfer by pipetting and does not redissolve into the supernatant. It strongly resembles a dense phase observed in LLPS (Alberti and Hyman 2021). During NMR experiments under MAS, the protein is centrifuged further to the rotor wall (Fig. 2b) due to the much higher g-force experienced than in the ultracentrifuge. After the measurements, we opened a rotor containing *Sf*T5 to assess the condition of the sample. A notable amount of gel was apparent on the rotor walls, as shown in Fig. S4. Nevertheless, the spectra obtained from this rotor did not change over a period of months, indicating that this state forms quickly at the start of the measurements through the effects of centrifugation. The fact that the protein gel is located at the rotor walls raises the question whether it is detected with slightly lower or higher sensitivity than sample in the center. In fact, the radial B<sub>1</sub> distribution appears very homogeneous for 0.7 mm rotors, with advantages for material at the rotor walls (Fig. S5).

With the outlined procedure, CP-based <sup>1</sup>H-<sup>15</sup>N correlation spectra with narrow lines are obtained (Fig. 2c). Importantly, no signs of an amorphous state or fibrils are observed, as could occur with desiccation of the sample. To avoid the latter, care must be taken to reduce water evaporation during spinning at the given temperature: rotor caps must either be tight enough, be glued into the rotor or be fitted with sealing plugs. High-quality spectra can then be acquired for at

**Fig. 2** Procedure for the preparation of sedimented samples. **(a)** Ultracentrifugation (UC) of the sample directly into the rotor using the tool shown in Fig. S2 and S3. The protein cartoon shown is a model of *Sa*ETF, with the two bound FAD molecules colored. **(b)** Development of the sample during measurements. **(c)**  $^1\text{H}$ - $^{15}\text{N}$  NMR correlation of  $^{13}\text{C}$ ,  $^{15}\text{N}$ -labelled *Sa*ETF recorded at 100 kHz MAS, 294 K, and a proton frequency of 900 MHz. **(d)** Slices from a similar spectrum as in (c) but recorded with 2048  $t_1$  increments for a spectral width of 142 ppm in the nitrogen dimension, taken at the indicated cross peak positions 1 and 2 along  $F_1$  ( $^{15}\text{N}$ )



least two weeks, but usually much longer if water loss is prevented.

### *Sulfolobus acidocaldarius* ETF

Many redox-active enzymes employ conformational changes to regulate electron transfer in accordance with substrate availability and access to partner proteins (Rees and Howard 1999; Huang et al. 2013). Moderately simple examples are electron transfer flavoproteins (ETFs), one of which mediates electron bifurcation in anaerobes, including archaea (Peters et al. 2016; Garcia Costas et al. 2017; Duan et al. 2018; Müller et al. 2018). *Sa*ETF has 609 amino acids and a molar mass of 67 kDa. It contains two flavin-adenine-dinucleotide (FAD) molecules, one bound in each of the two domains: one 14 kDa domain, termed the ‘head’, and another 53 kDa ‘base’ domain. In an attempt to understand structural rearrangements associated with catalysis, which is expected to involve an  $80^\circ$  rotation of the head domain (Toogood et al. 2005; Demmer et al. 2017; Murray et al. 2024), we plan to characterize structure and dynamics of this system by MAS NMR in further studies.

The sedimented samples yielded a well-resolved  $^1\text{H}$ - $^{15}\text{N}$  NMR correlation (Fig. 2c, d) by a CP-based pulse sequence (Paulson et al. 2003; Zhou and Rienstra 2008) at 100 kHz MAS, whose dispersed cross peaks overlay well with those of an INEPT-based  $^1\text{H}$ - $^{15}\text{N}$  HSQC spectrum (Bodenhausen and Ruben 1980) recorded on a deuterated sample in solution (Fig. 3a). The advantage of the CP-based approach is evident from the overlay (Fig. 3b), in that it visualizes numerous

signals that are not evident in the  $^1\text{H}$ - $^{15}\text{N}$  INEPT HSQC spectrum of the deuterated sample. This is most apparent from slices along  $F_1$  taken at 8.95 ppm  $^1\text{H}$  chemical shift as shown in Fig. S6. Most likely, these signals with chemical shifts characteristic of  $\beta$ -sheet structure are missing in the solution NMR spectrum owing to insufficient exchange of protons into backbone positions in *Sa*ETF expressed in 100%  $\text{D}_2\text{O}$ -containing medium.

Overall, the MAS NMR spectrum shows a large number of dispersed cross peaks that permit measurement of the line widths. In a CP-based  $^1\text{H}$ - $^{15}\text{N}$  correlation recorded with a spectral resolution of 12.6 Hz in  $t_1$  (2048  $t_1$  increments for 142 ppm), we observe a width at half-height of 20–30 Hz for nitrogen signals when processed without weighting functions (Fig. 2d, see also arrows in 2D spectrum, Fig. 2c). In the same spectrum, proton linewidths in the range of 150–300 Hz are observed. Minimal water loss occurred during the initial measurement sessions, as indicated by a comparison of 1D  $^1\text{H}$  spectra (Fig. S1), recorded on the fresh sample and one year later. These spectra revealed that the initial protein-to-water ratio roughly estimated to be approximately 1:2.5 (w/w) (see Fig. S1 and Materials and methods) only changed marginally over this period. Furthermore, the state of the sample remained largely the same, as indicated by a CP correlation recorded after one year (Fig. S7).

There is a striking difference in peak pattern between the CP-based (Fig. 4a) and INEPT (Fig. 4b)  $^1\text{H}$ - $^{15}\text{N}$  correlations, which indicates a residual overall motion of the protein (Aebischer and Ernst 2024). In a nutshell, at room temperature very rigid systems like  $\beta$ -sheets in protein crystals show

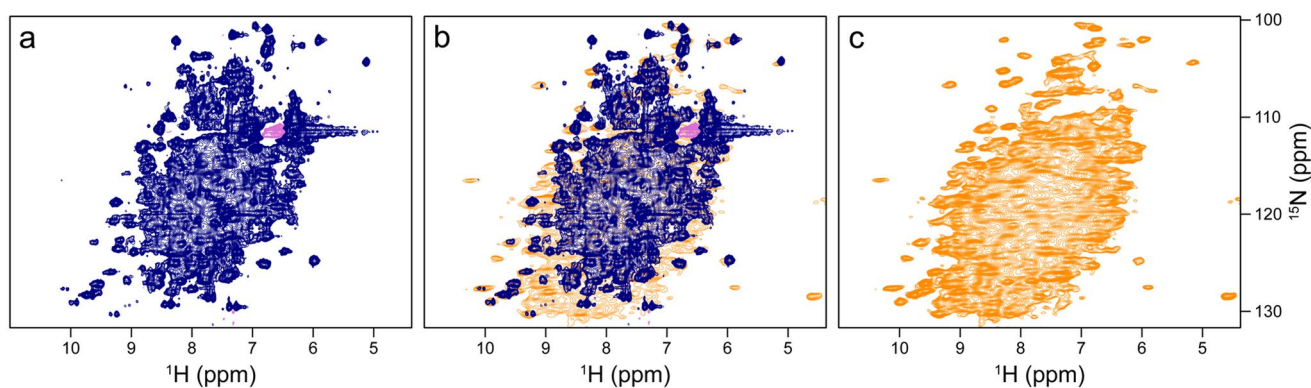


**Fig. 3** Comparison of the CP-based  $^1\text{H}$ - $^{15}\text{N}$  NMR correlation of non-deuterated *SaETF* shown in Fig. 2c with a corresponding solution NMR spectrum of a sample deuterated in the non-exchangeable sites. Both spectra were recorded at 900 MHz Larmor frequency. **(a)**  $^1\text{H}$ - $^{15}\text{N}$  N

HSQC of a dilute solution of  $^2\text{H}$ ,  $^{15}\text{N}$ -labelled *SaETF* (dark blue) **(b)** Overlay with the  $^1\text{H}$ - $^{15}\text{N}$  NMR correlation (orange) shown in Fig. 2c. **(c)** Spectrum shown in Fig. 2c, for comparison

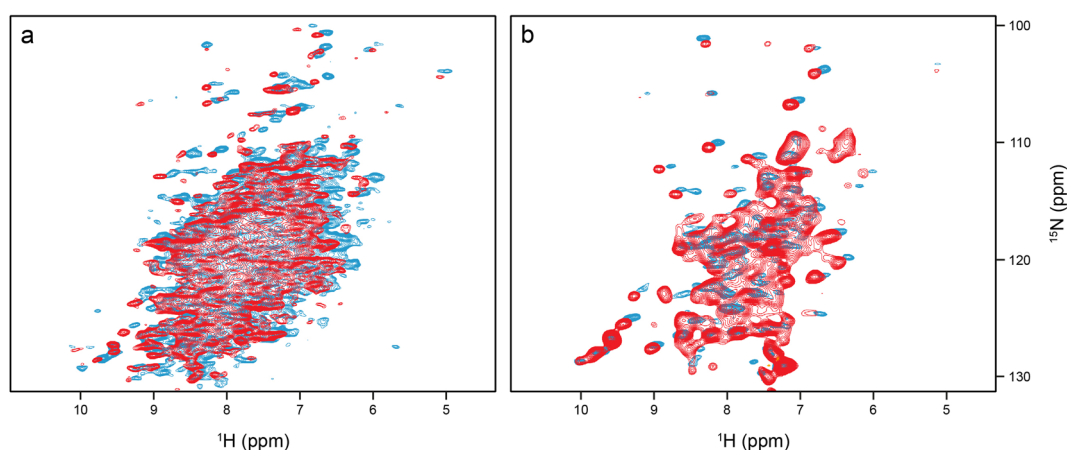


**Fig. 4** Comparison of CP-based **(a)** and INEPT-based **(b)**  $^1\text{H}$ - $^{15}\text{N}$  correlations of *SaETF* recorded at 289 and 313 K (blue and red, respectively), both under 100 kHz MAS and at 900 MHz proton Larmor frequency

signals with long  $T_2$  and hence with a narrow line width under MAS that appear in both, CP- and INEPT-based correlations. Mobile moieties like flexible termini do not show up in CP-based but INEPT correlations. There is an intermediate range where no INEPT transfers are observed, but where CP is already efficient. Most signals of folded protein moieties, even in a crystalline environment, fall into this latter category, reflecting some local motion. The quantitative aspects are nicely outlined in Aebischer and Ernst (Aebischer and Ernst 2024). Along these lines, the INEPT spectrum of *SaETF* shows only a subset of peaks with mostly random-coil chemical shifts, while the CP-based correlation gives the impression of a large protein with the expected dispersion. CP signal intensities were stronger at lower temperatures (see Fig. 4, blue 289 K and red 313 K). The high quality of the two spectra indicates that the protein molecules do not show the isotropic tumbling behavior observed in dilute solution, where transfers mediated by dipolar couplings are largely compromised. On the other hand, if the

system were completely rigid, the  $T_2$  times of all proton and nitrogen signals would be long enough at fast MAS to show the same cross peak patterns in Fig. 4b than those observed in Fig. 4a. In this case, a complete  $^1\text{H}$ - $^{15}\text{N}$  correlation would be expected *via* INEPT transfer. There is obviously considerable residual motion, in line with the observed absence of heterogeneous line broadening.

### Tryptophan synthase

*SrTS* consists of two  $\alpha$  (268 amino acids) and two  $\beta$  (397 amino acids) subunits. They assemble into an  $\alpha\beta\beta\alpha$  heterodimer with a total molecular weight of 144 kDa. While 126 X-ray structures are available in the PDB at the time of writing, knowledge of local mobility and conformational transitions, as well as the protonation states (particularly within the active site) (Caulkins et al. 2016; Holmes et al. 2022), is required to understand the catalytic cycle of the protein. Such factors are accessible by NMR after assigning



chemical shifts. In addition to the four-subunit *SrTS*, we also investigated isolated  $\beta$ -subunit dimers (*PfTrpB*, with a total molecular weight of 85 kDa). To estimate the prospects of obtaining resonance assignments on sedimented samples in each case, we recorded a set of representative 3D data sets for *SrTS* as well as the first scans of a series of different triple-resonance experiments for *PfTrpB*.

We first sedimented  $^{13}\text{C}$ ,  $^{15}\text{N}$ -labeled *SrTS* into a 0.7 mm rotor as described above and measured a CP-based  $^1\text{H}$ - $^{15}\text{N}$  correlation of which the NH region of the arginine residues is shown in Fig. 5a and the amide signal region in Fig. 5b. The resonance assignments (BMRB code 51,166 (Klein et al. 2022a) previously obtained from a crystalline sample (Klein et al. 2022b) are indicated by dots. Those assignments match for cross peaks with chemical shifts separate from the bulk signal conglomerate, which are the ones most affected by changes in local environment ( $\delta^1\text{H} > 9.7$  ppm;  $\delta^{15}\text{N} > 130$  ppm). Thus, the sedimented protein very likely retains the same structure as revealed by X-ray crystallography (Niks et al. 2013) and by NMR on a crystalline sample (Klein et al. 2022b).

As in the example before, we note more signals in the spectral region characteristic of  $\beta$ -sheets, between chemical shifts of 9.5 and 10.5 ppm  $^1\text{H}$ , than there are assignments indicated. The additional signals' most likely origins are the regions of the TIM barrel (Wu et al. 2007) buried inside the  $\alpha$  subunit that were previously unassigned. In order to test the feasibility of acquiring data sets suitable for resonance

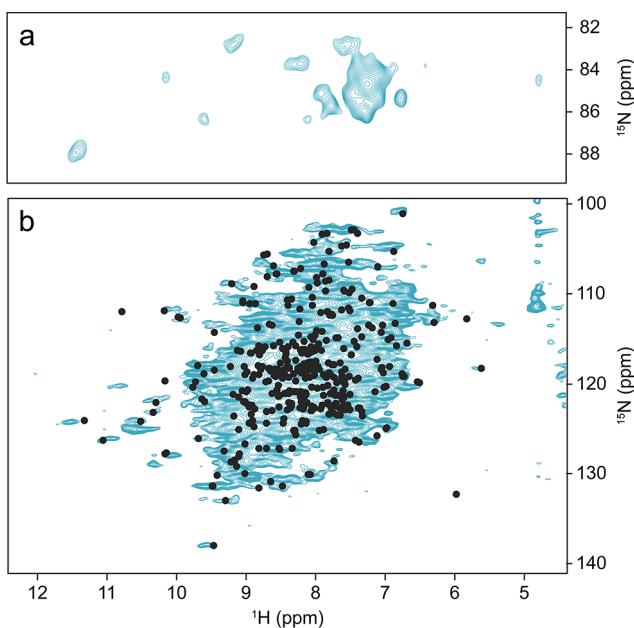


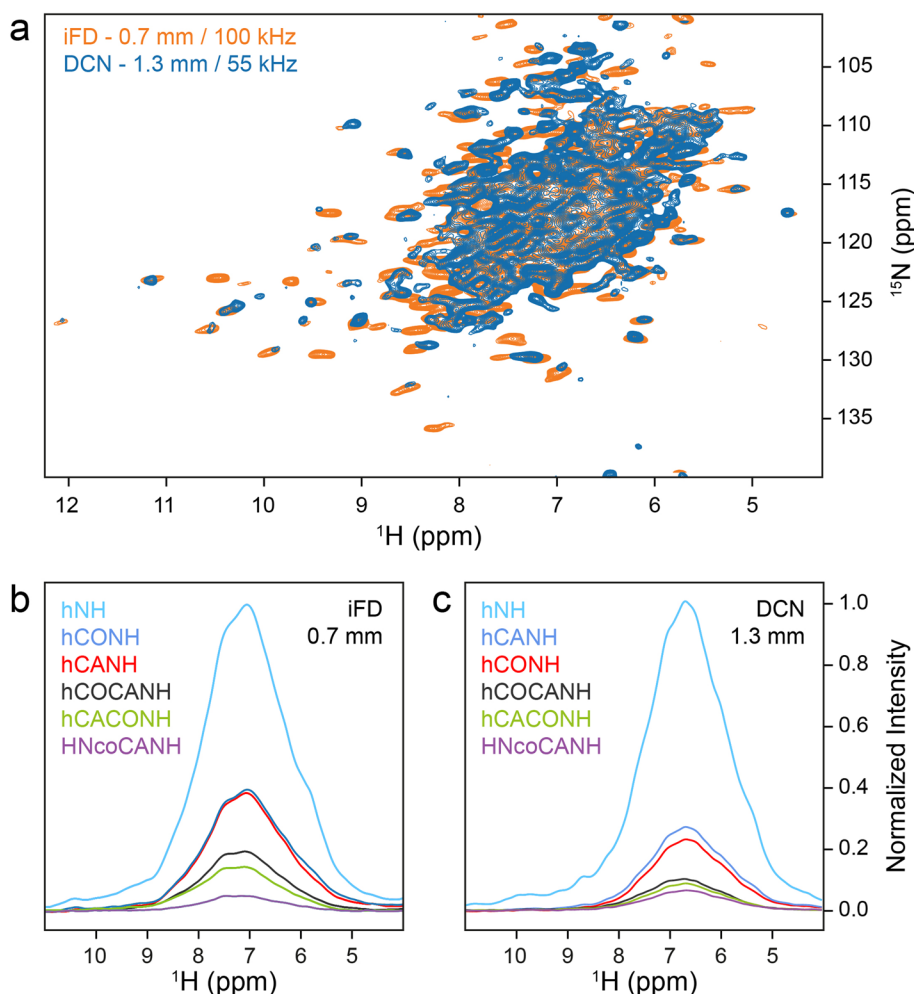
**Fig. 5** 2D CP-based  $^1\text{H}$ - $^{15}\text{N}$  NMR correlation recorded on fully protonated and  $^{13}\text{C}$ ,  $^{15}\text{N}$ -labelled *SrTS* in a 0.7 mm rotor at 100 kHz MAS. The black dots indicate the positions of assigned cross peaks (Klein et al. 2022a) (a) Arginine N $\epsilon$ H region of the spectrum. (b) Amide NH region

assignment, we recorded 3D hCONH and hCANH spectra (Fig. S8a, b for three-dimensional view and Fig. S8c, d for  $^1\text{H}$ - $^{13}\text{C}$  projections) (Barbet-Massin et al. 2014). The  $^1\text{H}$ - $^{15}\text{N}$  projections of the hCONH and hCANH spectra (Fig. S8e, f) match the 2D  $^1\text{H}$ - $^{15}\text{N}$  correlation. The two spectra each contain only one set of signals, indicating sample stability over the time of measurement. Altogether, this opens a different, more comprehensive avenue for sequence-specific resonance assignments and collection of structural constraints. As an additional advantage of fully protonated samples investigated at 100 kHz MAS, the CP-based  $^1\text{H}$ - $^{13}\text{C}$  correlation (Fig. S9) provides access to  $^1\text{H}$  chemical shifts of the side chains.

The molecular weight of *SrTS* is already large (144 kDa), making ultracentrifugation and MAS effective. To assess the prospects of sedimented samples for future studies, we used the *PfTrpB* sample comprising  $\beta$ -subunit dimers to compare the relative intensities of the first FID (i.e., their relative HN bulk intensities) of NMR data recorded with more complex pulse sequences that are useful for backbone resonance assignment. First, we used uniformly  $^{13}\text{C}$ ,  $^{15}\text{N}$ -labeled sediment, spun at 100 kHz MAS, with the protonation content tuned according to the iFD protocol ( $\text{H}_2\text{O}$ -based medium with deuterated glucose) to assure full protonation at amide sites while introducing a high degree of side chain deuteration (Medeiros-Silva et al. 2016). For comparison, a perdeuterated and back-exchanged sediment of *PfTrpB* was prepared. Again, a well-resolved spectrum is obtained at 100 kHz MAS, with additional cross peaks observed for the iFD sample in comparison to the spectrum of the perdeuterated sample recorded at 55 kHz MAS (Fig. 6a). We then recorded for both  $\beta$ -subunit samples 1D bulk amide proton signals from hNH, hCANH, hCONH, hCOCANH, hCACANH, and HNcoCANH experiments (Klein et al. 2022b), and compared bulk intensities within the sets (Fig. 6b and c). Relative to the hNH experiment, we obtained more intense signals for the 3D sequences in case of the iFD sample in the 0.7 mm rotor at 100 kHz MAS, which can be ascribed to higher start magnetization from the more abundant proton bath, rather than better transfer efficiencies compared to the triple labelled sample in the 1.3 mm rotor. However, the advantage of the iFD sample decreases for the most complex sequence employed (Fig. 6b and c, HNcoCANH), probably due to less efficient CP transfers at high MAS frequencies. For separate plots with percentages see Fig. S10.

A special opportunity for studying protein function is offered by the presence of arginine head group signals in a characteristic region of the  $^1\text{H}$ - $^{15}\text{N}$  NMR correlation (Fig. 5a). In the case of *SrTS*, R141 of the  $\beta$ -subunits is critically important for activity. It plays an essential role in stabilizing the closed form of the subunit by forming a salt

**Fig. 6** Comparison of spectra recorded on sedimented *PfTrpB* (~85 kDa) at 700 MHz  $^1\text{H}$  Larmor frequency. **(a)** Superposition of 2D  $^1\text{H}$ - $^{15}\text{N}$  NMR correlations of iFD-labeled *PfTrpB* in a 0.7 mm rotor (orange) and of  $^2\text{H}$ ,  $^{13}\text{C}$ ,  $^{15}\text{N}$ -labeled *PfTrpB* in a 1.3 mm rotor (blue), both sedimented under comparable conditions. **(b)** Ratios of bulk intensities obtained from the first increment of the indicated 2D, 3D or higher-dimensionality experiments recorded at 100 kHz. The colors of the spectra refer to the indicated 2D and 3D NMR experiments indicated to the left. **(c)** The same ratios for the deuterated sediment in a 1.3 mm rotor spinning at 55 kHz. Sequences and parameters used are similar to Klein et al. (Klein et al. 2022b). For parameters used see SI. Color code as in (c)



bridge with D305 upon substrate binding. Furthermore, it is part of the larger COMM domain ( $\beta$ 102- $\beta$ 189) involved in the allosteric regulation of the catalytic activities of the  $\alpha$ - and  $\beta$ -subunits (Schneider et al. 1998; Ghosh et al. 2022). The corresponding side chain signals may be resolved in this less crowded area of the spectrum and assigned by mutation.

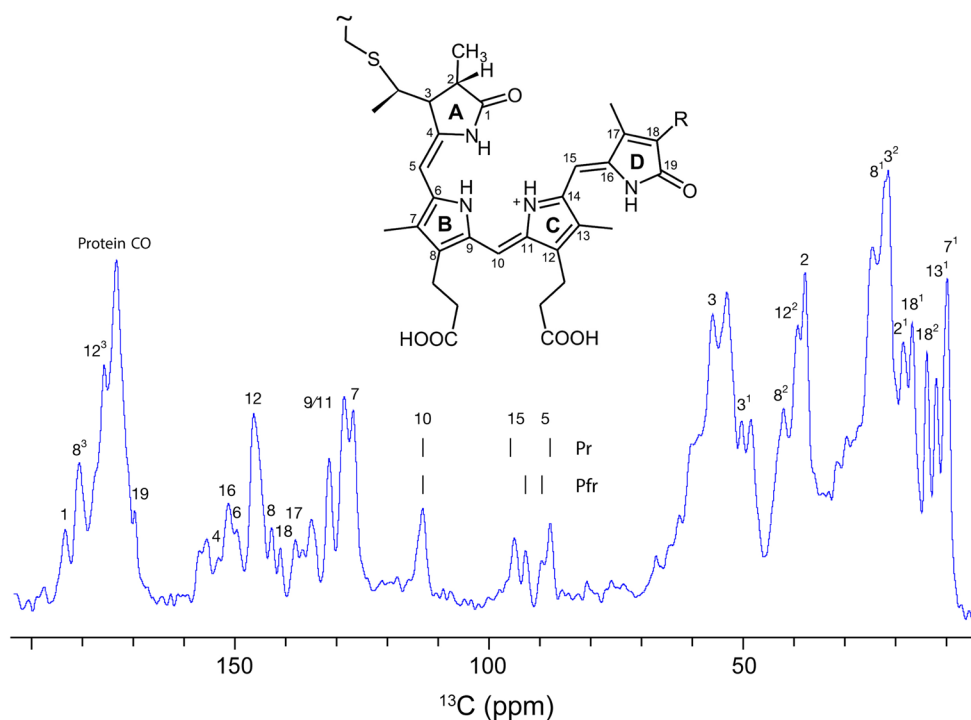
### Phytochrome Cph1 and a path to low-glycerol DNP samples

DNP NMR samples of the sensory module of the cyanobacterial phytochrome Cph1 (Rockwell et al. 2006; Essen et al. 2008; Hughes 2010) were prepared for two purposes: (i) to investigate potential exchange broadening of its chromophore carbon signals in measurements at room temperature that could occur analogously to previously detected amide  $^{15}\text{N}$  signal broadening (Hahn et al. 2008) and (ii) to assess the quality of DNP NMR samples prepared with minimal glycerol content. In both cases, the light-sensitive protein was investigated in 1.9 mm rotors. Here, the preparation

of a gel-like phase by ultracentrifugation, following earlier work by Ravera et al. (Ravera et al. 2013, 2014), was seen as an opportunity to reduce the amount of glycerol in DNP NMR samples that was added in a small amount after sedimentation.

A 1.0 mM Cph1 sample, with  $^{13}\text{C}$ ,  $^{15}\text{N}$  labelling exclusively in the phycocyanobilin chromophore, was sedimented into a 1.9 mm rotor. The 1D  $^{13}\text{C}$  NMR spectrum showed well-resolved signals for methine carbons C5, C10, and C15 (inset of Fig. 7), at the expected chemical shift positions, and similar linewidths for all signals. Exchange broadening due to ring reorientation or other alterations in the double-bond network due to protonation/deprotonation events were not apparent (Fig. 7). In those measurements, the signal-to-noise ratio (S/N) was low necessitating several hours of acquisition, presumably due to low protein concentration. In fact, after centrifugation, the sample remained oily, less gel-like, indicating a more dilute aqueous phase loaded into the rotor from which a gel, containing less protein, is formed upon MAS.

**Fig. 7** 1D  $^{13}\text{C}$  NMR spectrum of the sedimented phytochrome Cph1 solely labeled in its chromophore (PCB, inset), recorded at 261 K and 20 kHz MAS at a field of 18.8 T



A similar sample of Cph1 but with amino-acid selective  $^{13}\text{C}$ ,  $^{15}\text{N}$  labelling of Ile, Arg, Val and Trp was prepared for DNP measurements from a 1.7 mM solution, to which the radical bcTolM dissolved in  $d_8$ -glycerol was added, so that the final glycerol concentration in the buffer was low (11%  $d_8$ -glycerol/22%  $\text{D}_2\text{O}$ /67%  $\text{H}_2\text{O}$ ; v/v). This sample showed substantial 20-fold Boltzmann enhancements (Fig. S11), enabling collection of complex 3D hCANcoCA spectra (Chevelkov et al. 2013) with sufficiently good S/N in 4.5 days at a  $^1\text{H}$  NMR frequency of 800 MHz. Here, the substantial Boltzmann enhancement at 105 K indicates that freeze concentration of polarizing agent was suppressed despite the low glycerol concentration.

### Concluding remarks

Here, we report parameters, procedures and tools for sedimenting proteins in a molecular weight range between 40 and 140 kDa into MAS rotors in order to record well-resolved  $^1\text{H}$ - $^{15}\text{N}$  correlations and sets of 3D spectra. By means of the outlined procedure, a dense phase is produced whose NMR spectra do not show noticeable heterogeneous broadening, thus exhibiting a liquid-like appearance apart from the larger line width. Yet, CP provides an efficient magnetization transfer mechanism. In the case of *Sa*ETF we showed that the water-to-protein-ratio is 1:2.5 (w/w) and remains stable over time, with very similar spectra obtained after one year. Structural integrity of the sedimented proteins was demonstrated by comparison of the CP-based  $^1\text{H}$ - $^{15}\text{N}$  correlation spectra recorded on the dense phases with

solution  $^1\text{H}$ - $^{15}\text{N}$  HSQC spectra or CP-based correlations obtained from crystalline samples. Although the much narrower line width in the CP-based 2D-spectra of the crystalline TS sample nurture the expectation of a better signal to noise as compared to the spectra of the sedimented sample, the S/N in spectra of the iFD labeled sample of *Pf*TrpB is sufficient to enable assignment procedures.

Here, dense phases of folded proteins are generated by ultracentrifugation. In LLPS, similar dense phases occur, yet of mostly unstructured proteins, following suitable changes of buffer conditions. Those dense phases form spontaneously after induction of LLPS and tend to develop rapidly towards fibrillar states, often involving short repeats in their amino acid sequence (Alberti and Hyman 2021). In principle, one could expect such tendency to form fibrils to be a problem of our approach. However, the dense phases of well-folded, globular proteins produced by ultracentrifugation did not show signs of fibrils even after weeks, as demonstrated by the set of clean 3D spectra obtained on *Sf*TS (Fig. S8) or by the long-term *Sa*ETF spectrum shown in Fig. S7, all being consistent with previous observations (Wiegand et al. 2020).

Among the factors influencing sensitivity, lower temperature helps to increase S/N in CP-based experiments.  $^1\text{H}$ - $^{15}\text{N}$  correlation spectra obtained after sedimentation show overall good resolution in the proton dimension (150–300 Hz at 100 kHz MAS), and excellent resolution in the nitrogen dimension. The nitrogen line widths of 20–30 Hz observed in spectra of *Sa*ETF already indicates that the use of TROP-like sequences that exploit both, dipolar and scalar

couplings for C-N transfer may be advantageous (Blahut et al. 2022).

The approach presented here contrasts the originally proposed FROSTY technique (Mainz et al. 2009). There, it was proposed that it is beneficial to use buffers containing 20% glycerol with the argument that this could reduce molecular tumbling due to the higher viscosity of the solvent mixture. From our perspective it needs to be considered that glycerol is more dense than pure water, as are glycerol/water mixtures, which may potentially interfere with the formation of a dense phase by centrifugation. The density of an 80% water / 20% glycerol mixture (w/w) is 1.048 at 15 °C. As an example for a dense protein phase we may consider egg white whose density ranges between 1.02 and 1.1. In such a situation it may happen that the sedimentation process is disturbed by glycerol.

The investigation of protein sediments instead of crystalline preparations may be advantageous when additives are required for crystallization that cannot easily be deuterated or carbon-depleted. Furthermore, there is larger freedom in the choice of pH and other buffer conditions than typically required for crystallization. In particular, this may facilitate NMR studies on complexes of drug targets with small molecule inhibitors or activators at appropriate conditions. The slightly larger line width observed in spectra of dense phases than in spectra of crystalline samples will be a case-specific tradeoff vs. the larger experimental freedom. Our approach also has advantages compared to solution NMR in that no deuteration of the protein is required when spinning the sample at 100 kHz MAS and above. A complete set of signals can thus be obtained. It has further value when cells of higher organisms than bacteria or yeast are employed as expression hosts, since complete deuteration cannot be achieved in this case.

It was demonstrated by Wiegand et al. that protein-DNA and protein-RNA complexes remain stable under fast MAS conditions (Wiegand et al. 2020). Considering the special advantage that deuteration can be avoided and that non-exchangeable protons can aid assignment procedures and enrich functional studies, we expect a particularly high impact of the presented approach on the investigation of RNA and their complexes. Those complexes are difficult to crystallize, there is yet no possibility to predict satisfying three-dimensional structures of them, and deuteration of RNA is costly. Additionally, the dispersion of the chemical shifts of nucleic acid aromatic protons and of sugar anomeric protons is high and may aid in assignment procedures. Furthermore, desired sections of the RNA may be selectively  $^{13}\text{C}$ ,  $^{15}\text{N}$ -labelled so that spectra become less crowded.

The possibility of obtaining extended data sets with well-resolved spectra of sedimented proteins has far-reaching

consequences regarding the current paradigm of NMR. Soluble proteins of 40–110 kDa in size that were currently not easily tractable by solution NMR are now accessible with the help of MAS NMR methods. Proteins and their complexes in this size range are also not easy to tackle by cryo-electron microscopy at the current state of technology, so that MAS NMR on sedimented samples may play a special role in structural biology. As a bonus, proton signals may be detected and  $^1\text{H}$ -chemical shifts may help to disperse spectra and to collect structural restraints. The possibility to detect exchangeable protons enables mechanistic studies.

**Supplementary Information** The online version contains supplementary material available at <https://doi.org/10.1007/s10858-024-00444-9>.

**Acknowledgements** This work was supported by the Einstein Foundation, Berlin (A.F.M. and D.M.B.). The authors are grateful to Dr. Martin Bommer (Max-Delbrück-Center, 13125 Berlin, Germany) for providing the molecular cloning kit for *Sa*ETF, and to Nina Schröder and Thomas Wiegand for sedimentation of a *P/TrpB* sample. H.O. and J.H. acknowledge support by the *Deutsche Forschungsgemeinschaft* (DFG, German Research Foundation) within SFB 1078 and the grants OS 106/17–1 (H.O.) and HU 702/12–1 (J.H.). D.M.B. and A.-F. M. acknowledge support from the Einstein Foundation of Berlin, EVF-2019-503-2. L.J.M. acknowledges grant support from the US National Institutes of Health (R01GM137008, R35GM145369). R.L. acknowledges funding by the DFG under Germany's Excellence Strategy - EXC 2033–390677874 – RESOLV and further by the European Union (ERC, 101082494 *bypassNMR*). Views and opinions expressed are however those of the author(s) only and do not necessarily reflect those of the European Union or the European Research Council. Neither the European Union nor the granting authority can be held responsible for them.

**Author contributions** A.F.M., L.J.M., R.L. and H.O. designed research; D. B., F. L., L. G., H. A., A. K., D. F., D. H., K. G., T. M., A. D. performed research; D. B., F. L., L. G., H. A., A. K., D. F., M. H., K. G., A. D., J. H., L. J. M., R. L., (A) F. M. and H.O. analyzed data; and F. L., (B) v. R., J. H., L. J. M., R. L., A. F. M. and H.O. wrote the paper.

**Funding** Open Access funding enabled and organized by Projekt DEAL.

**Data availability** No datasets were generated or analysed during the current study.

## Declarations

**Competing interests** The authors declare no competing interests.

**Open Access** This article is licensed under a Creative Commons Attribution 4.0 International License, which permits use, sharing, adaptation, distribution and reproduction in any medium or format, as long as you give appropriate credit to the original author(s) and the source, provide a link to the Creative Commons licence, and indicate if changes were made. The images or other third party material in this article are included in the article's Creative Commons licence, unless indicated otherwise in a credit line to the material. If material is not included in the article's Creative Commons licence and your intended use is not permitted by statutory regulation or exceeds the permitted



use, you will need to obtain permission directly from the copyright holder. To view a copy of this licence, visit <http://creativecommons.org/licenses/by/4.0/>.

## References

- Aebischer K, Ernst M (2024) INEPT and CP transfer efficiencies of dynamic systems in MAS solid-state NMR. *J Magn Reson* 359:107617. <https://doi.org/10.1016/j.jmr.2024.107617>
- Alberti S, Hyman AA (2021) Biomolecular condensates at the nexus of cellular stress, protein aggregation disease and ageing. *Nat Rev Mol Cell Biol* 22:196–213. <https://doi.org/10.1038/s41580-020-00326-6>
- Barbet-Massin E, Pell AJ, Retel JS et al (2014) Rapid Proton-detected NMR assignment for proteins with fast Magic Angle Spinning. *J Am Chem Soc* 136:12489–12497. <https://doi.org/10.1021/ja507382j>
- Barnes AB, De Paëpe G, Van Der Wel PCA et al (2008) High-field Dynamic Nuclear polarization for solid and Solution Biological NMR. *Appl Magn Reson* 34:237–263. <https://doi.org/10.1007/s00723-008-0129-1>
- Bertini I, Luchinat C, Parigi G et al (2011) Solid-state NMR of proteins sedimented by ultracentrifugation. *Proc Natl Acad Sci USA* 108:10396–10399. <https://doi.org/10.1073/pnas.1103854108>
- Bertini I, Engelke F, Luchinat C et al (2012) NMR properties of sedimented solutes. *Phys Chem Chem Phys* 14:439–447. <https://doi.org/10.1039/C1CP22978H>
- Bertini I, Luchinat C, Parigi G, Ravera E (2013) SedNMR: on the edge between solution and solid-state NMR. *Acc Chem Res* 46:2059–2069. <https://doi.org/10.1021/ar300342f>
- Blahut J, Brandl MJ, Pradhan T et al (2022) Sensitivity-enhanced Multidimensional solid-state NMR spectroscopy by optimal-control-based transverse mixing sequences. *J Am Chem Soc* 144:17336–17340. <https://doi.org/10.1021/jacs.2c06568>
- Bodenhausen G, Ruben DJ (1980) Natural abundance nitrogen-15 NMR by enhanced heteronuclear spectroscopy. *Chem Phys Lett* 69:185–189. [https://doi.org/10.1016/0009-2614\(80\)80041-8](https://doi.org/10.1016/0009-2614(80)80041-8)
- Bolik-Coulon N, Sever AIM, Harkness RW et al (2023) Less is more: a simple methyl-TROSY based pulse scheme offers improved sensitivity in applications to high molecular weight complexes. *J Magn Reson* 346:107326. <https://doi.org/10.1016/j.jmr.2022.107326>
- Buller AR, Brinkmann-Chen S, Romney DK et al (2015) Directed evolution of the tryptophan synthase  $\beta$ -subunit for stand-alone function recapitulates allosteric activation. *Proc Natl Acad Sci USA* 112:14599–14604. <https://doi.org/10.1073/pnas.1516401112>
- Caulkins BG, Young RP, Kudla RA et al (2016) NMR crystallography of a Carbanionic Intermediate in Tryptophan synthase: Chemical structure, tautomerization, and reaction specificity. *J Am Chem Soc* 138:15214–15226. <https://doi.org/10.1021/jacs.6b08937>
- Chevelkov V, Shi C, Fasshuber HK et al (2013) Efficient band-selective homonuclear CO–CA cross-polarization in protonated proteins. *J Biomol NMR* 56:303–311. <https://doi.org/10.1007/s10858-013-9767-1>
- Demmer JK, Pal Chowdhury N, Selmer T et al (2017) The semiquinone swing in the bifurcating electron transferring flavoprotein/butyryl-CoA dehydrogenase complex from *Clostridium difficile*. *Nat Commun* 8:1577. <https://doi.org/10.1038/s41467-017-01746-3>
- Duan HD, Lubner CE, Tokmina-Lukaszewska M et al (2018) Distinct properties underlie flavin-based electron bifurcation in a novel electron transfer flavoprotein FixAB from *Rhodospseudomonas palustris*. *J Biol Chem* 293:4688–4701. <https://doi.org/10.1074/jbc.RA117.000707>
- Essen L-O, Mailliet J, Hughes J (2008) The structure of a complete phytochrome sensory module in the pr ground state. *Proc Natl Acad Sci USA* 105:14709–14714. <https://doi.org/10.1073/pnas.0806477105>
- Fragai M, Luchinat C, Parigi G, Ravera E (2013) Practical considerations over spectral quality in solid state NMR spectroscopy of soluble proteins. *J Biomol NMR* 57:155–166. <https://doi.org/10.1007/s10858-013-9776-0>
- Fung BM, Khittrik AK, Ermolaev K (2000) An Improved Broadband Decoupling sequence for liquid crystals and solids. *J Magn Reson* 142:97–101. <https://doi.org/10.1006/jmre.1999.1896>
- Garcia Costas AM, Poudel S, Miller A-F et al (2017) Defining Electron Bifurcation in the Electron-transferring Flavoprotein Family. *J Bacteriol* 199. <https://doi.org/10.1128/JB.00440-17>
- Ghosh RK, Hilario E, Chang CA et al (2022) Allosteric regulation of substrate channeling: *Salmonella typhimurium* tryptophan synthase. *Front Mol Biosci* 9:923042. <https://doi.org/10.3389/fmolb.2022.923042>
- Gronenborn AM (2022) Small, but powerful and attractive: 19F in biomolecular NMR. *Structure* 30:6–14. <https://doi.org/10.1016/j.str.2021.09.009>
- Hahn J, Strauss HM, Schmieder P (2008) Heteronuclear NMR investigation on the structure and Dynamics of the Chromophore binding Pocket of the Cyanobacterial Phytochrome Cph1. *J Am Chem Soc* 130:11170–11178. <https://doi.org/10.1021/ja8031086>
- Hall DA, Maus DC, Gerfen GJ et al (1997) Polarization-enhanced NMR spectroscopy of Biomolecules in Frozen Solution. *Science* 276:930–932. <https://doi.org/10.1126/science.276.5314.930>
- Hoch JC, Baskaran K, Burr H et al (2023) Biological Magnetic Resonance Data Bank. *Nucleic Acids Res* 51:D368–D376. <https://doi.org/10.1093/nar/gkac1050>
- Holmes JB, Liu V, Caulkins BG et al (2022) Imaging active site chemistry and protonation states: NMR crystallography of the tryptophan synthase  $\alpha$ -aminoacrylate intermediate. *Proc Natl Acad Sci USA* 119:e2109235119. <https://doi.org/10.1073/pnas.2109235119>
- Huang W-C, Ellis J, Moody PCE et al (2013) Redox-Linked Domain movements in the Catalytic cycle of cytochrome P450 reductase. *Structure* 21:1581–1589. <https://doi.org/10.1016/j.str.2013.06.022>
- Huestis WH, Raftery MA (1975) Conformation and cooperativity in hemoglobin. *Biochemistry* 14:1886–1892. <https://doi.org/10.1021/bi00680a013>
- Hughes J (2010) Phytochrome three-dimensional structures and functions. *Biochem Soc Trans* 38:710–716. <https://doi.org/10.1042/BST0380710>
- Jehle S, Rajagopal P, Bardiaux B et al (2010) Solid-state NMR and SAXS studies provide a structural basis for the activation of  $\alpha$ B-crystallin oligomers. *Nat Struct Mol Biol* 17:1037–1042. <https://doi.org/10.1038/nsmb.1891>
- Jumper J, Evans R, Pritzel A et al (2021) Highly accurate protein structure prediction with AlphaFold. *Nature* 596:583–589. <https://doi.org/10.1038/s41586-021-03819-2>
- Klein A, Rovó P, Sakhrani VV et al (2022a) Solid-state NMR assignments of tryptophan synthase of *S. typhimurium*. <https://doi.org/10.13018/BMR51166>. Biological Magnetic Resonance Data Bank
- Klein A, Rovó P, Sakhrani VV et al (2022b) Atomic-resolution chemical characterization of (2x)72-kDa tryptophan synthase via four- and five-dimensional  $^1$ H-detected solid-state NMR. *Proc Natl Acad Sci USA* 119:e2114690119. <https://doi.org/10.1073/pnas.2114690119>
- Klukowski P, Riek R, Güntert P (2023) NMRtist: an online platform for automated biomolecular NMR spectra analysis. *Bioinformatics* 39:btad066. <https://doi.org/10.1093/bioinformatics/btad066>

- Loquet A, Sgourakis NG, Gupta R et al (2012) Atomic model of the type III secretion system needle. *Nature* 486:276–279. <https://doi.org/10.1038/nature11079>
- Luck LA, Falke JJ (1991) Open conformation of a substrate-binding cleft: fluorine-19 NMR studies of cleft angle in the D-galactose chemosensory receptor. *Biochemistry* 30:6484–6490. <https://doi.org/10.1021/bi00240a019>
- Mainz A, Jehle S, Van Rossum BJ et al (2009) Large protein complexes with Extreme Rotational Correlation Times Investigated in solution by Magic-Angle-spinning NMR spectroscopy. *J Am Chem Soc* 131:15968–15969. <https://doi.org/10.1021/ja904733v>
- Medeiros-Silva J, Mance D, Daniëls M et al (2016) 1 H-Detected solid-state NMR studies of Water-Inaccessible proteins in Vitro and in situ. *Angew Chem Int Ed* 55:13606–13610. <https://doi.org/10.1002/anie.201606594>
- Müller V, Chowdhury NP, Basen M (2018) Electron Bifurcation: a long-hidden energy-coupling mechanism. *Annu Rev Microbiol* 72:331–353. <https://doi.org/10.1146/annurev-micro-090816-093440>
- Murray DT, Ge X, Schut GJ et al (2024) Correlating Conformational Equilibria with Catalysis in the Electron Bifurcating EtfABCX of *Thermotoga maritima*. *Biochemistry* 63:128–140. <https://doi.org/10.1021/acs.biochem.3c00472>
- Niks D, Hilario E, Dierkers A et al (2013) Allostery and substrate channeling in the Tryptophan synthase Bifunctional Complex: evidence for two subunit conformations and four Quaternary States. *Biochemistry* 52:6396–6411. <https://doi.org/10.1021/bi400795e>
- Paulson EK, Morcombe CR, Gaponenko V et al (2003) Sensitive high resolution inverse detection NMR spectroscopy of proteins in the solid state. *J Am Chem Soc* 125:15831–15836. <https://doi.org/10.1021/ja037315+>
- Peters JW, Miller A-F, Jones AK et al (2016) Electron bifurcation. *Curr Opin Chem Biol* 31:146–152. <https://doi.org/10.1016/j.cbpa.2016.03.007>
- Ravera E, Corzilius B, Michaelis VK et al (2013) Dynamic nuclear polarization of sedimented solutes. *J Am Chem Soc* 135:1641–1644. <https://doi.org/10.1021/ja312553b>
- Ravera E, Corzilius B, Michaelis VK et al (2014) DNP-Enhanced MAS NMR of bovine serum albumin sediments and solutions. *J Phys Chem B* 118:2957–2965. <https://doi.org/10.1021/jp500016f>
- Rees DC, Howard JB (1999) Structural bioenergetics and energy transduction mechanisms. *J Mol Biol* 293:343–350. <https://doi.org/10.1006/jmbi.1999.3005>
- Retel JS, Nieuwkoop AJ, Hiller M et al (2017) Structure of outer membrane protein G in lipid bilayers. *Nat Commun*. <https://doi.org/10.1038/s41467-017-02228-2>. 8:2073
- Rockwell NC, Su Y-S, Lagarias JC (2006) Phytochrome structure and signaling mechanisms. *Annu Rev Plant Biol* 57:837–858. <https://doi.org/10.1146/annurev.arplant.56.032604.144208>
- Sarkar R, Mainz A, Busi B et al (2016) Immobilization of soluble protein complexes in MAS solid-state NMR: Sedimentation versus viscosity. *Solid State Nucl Magn Reson* 76–77:7–14. <https://doi.org/10.1016/j.ssnmr.2016.03.005>
- Schneider TR, Gerhardt E, Lee M et al (1998) Loop Closure and Inter-subunit Communication in Tryptophan Synthase. *Biochemistry* 37:5394–5406. <https://doi.org/10.1021/bi9728957>
- Stöppler D, Oschkinat H (2018)  $^1\text{H}$ ,  $^{13}\text{C}$ ,  $^{13}\text{C}$ B and  $^{15}\text{N}$  chemical shift assignments of b2-microglobulin and a-chain of the neonatal fc receptor. <https://doi.org/10.13018/BMR27437>. Biological Magnetic Resonance Data Bank
- Stöppler D, Macpherson A, Smith-Penzel S et al (2018) Insight into small molecule binding to the neonatal fc receptor by X-ray crystallography and 100 kHz magic-angle-spinning NMR. *PLoS Biol* 16:e2006192. <https://doi.org/10.1371/journal.pbio.2006192>
- Toogood HS, Van Thiel A, Scrutton NS, Leys D (2005) Stabilization of non-productive conformations underpins Rapid Electron Transfer to Electron-transferring Flavoprotein. *J Biol Chem* 280:30361–30366. <https://doi.org/10.1074/jbc.M505562200>
- Tugarinov V, Hwang PM, Ollerenshaw JE, Kay LE (2003) Cross-correlated relaxation enhanced  $^1\text{H}$ – $^{13}\text{C}$  NMR spectroscopy of Methyl Groups in very high Molecular Weight proteins and protein complexes. *J Am Chem Soc* 125:10420–10428. <https://doi.org/10.1021/ja030153x>
- Wiegand T, Lacabanne D, Torosyan A et al (2020) Sedimentation yields long-term stable protein samples as shown by solid-state NMR. *Front Mol Biosci* 7:17. <https://doi.org/10.3389/fmolb.2020.00017>
- Wu Y, Vadrevu R, Kathuria S et al (2007) A tightly packed hydrophobic cluster directs the formation of an off-pathway sub-millisecond folding Intermediate in the  $\alpha$  subunit of Tryptophan Synthase, a TIM Barrel protein. *J Mol Biol* 366:1624–1638. <https://doi.org/10.1016/j.jmb.2006.12.005>
- Zhou DH, Rienstra CM (2008) High-performance solvent suppression for Proton detected solid-state NMR. *J Magn Reson* 192:167–172. <https://doi.org/10.1016/j.jmr.2008.01.012>

**Publisher's Note** Springer Nature remains neutral with regard to jurisdictional claims in published maps and institutional affiliations.